IEEE Access
Multidisciplinary | Rapid Review | Open Access Journal

Received 27 March 2026, accepted 28 April 2026, date of publication 4 May 2026, date of current version 8 May 2026.

Digital Object Identifier 10.1109/ACCESS.2026.3690017

RESEARCH ARTICLE

Real-Time Automatic Train Regulation of Metro Lines With Bifurcations and Short-Turning Under Continuous Communication

ÁLVARO CIDONCHA[1], ADRIÁN FERNÁNDEZ-RODRÍGUEZ[1], ASUNCIÓN P. CUCALA[1], ANTONIO FERNÁNDEZ-CARDADOR[1], AND JORGE GOROSTIZA-HERRERO[2]

[1]Institute for Research in Technology, ICAI School of Engineering, Comillas Pontifical University, 28015 Madrid, Spain
[2]Mass Transit Business Unit, CAF Signalling, Amorebieta-Etxano, 48340 Biscay, Spain

Corresponding author: Adrián Fernández-Rodríguez (adrian.fernandez@iit.comillas.edu)

This work was supported in part by European Union, and in part by the Project "Flagship Project 1: Network Management Planning and Control and Mobility Management in a Multimodal Environment and Digital Enablers (FP1-MOTIONAL)" through Europe's Rail Joint Undertaking and its members.

ABSTRACT This paper introduces a novel Real-Time Model Predictive Control (MPC) framework for automatic train regulation in complex metro lines featuring bifurcations, short-turning operations, and continuous communication systems (CBTC or ERTMS), enabling real-time information exchange between trains and control centers for traffic supervision and control. This framework addresses a critical gap in existing approaches: enabling the restoration of nominal operations after moderate disruptions when the line is not limited to a simple or looped infrastructure. The proposed approach operates in two stages: first, a predictive mathematical algorithm generates running-time and dwell-time control actions, balancing timetable adherence and headway regularity subject to topological constraints. Second, these actions are processed by a module that generates real-time automatic driving commands. A key contribution is the incorporation of a granular optimization strategy that enhances energy efficiency while preserving operational performance. The algorithm was validated on a simulation platform based on a real Spanish metro line and, compared to traditional regulation, the results demonstrate a 30.00% improvement in headway adherence and a 7.80% reduction in passenger waiting time in high-demand areas, along with a 10.37% reduction in energy consumption. The computational efficiency of the proposed model confirms its suitability for real-time application in large-scale, complex transit infrastructures.

INDEX TERMS Automatic train regulation, complex topology, energy efficiency, mass transit systems, model predictive control, real-time optimization.

I. INTRODUCTION

In recent decades, urban rail systems have become a key component of sustainable mobility due to their high capacity, energy efficiency, and low environmental impact. However, increasing urbanization has intensified demand, requiring more reliable and efficient operations. Automatic Train Operation (ATO) addresses this by executing driving commands such as acceleration, braking, and platform stops, thereby improving punctuality, capacity, and passenger comfort [1].

The use of ATO also allows for the creation of pre-designed schedules at the start of operations. In [2], a model based on dynamic programming is proposed for designing such a schedule through speed profiles specifically developed for energy savings while meeting a predefined line travel time.

However, even with ATO, in high-frequency services, minor and moderate disruptions such as boarding delays or technical issues can cause cascading effects, impacting the entire line and leading to delays and congestion [3]. In addition to these internal sources of disturbance, external factors such as adverse weather conditions can also significantly affect railway operations [4].

The associate editor coordinating the review of this manuscript and approving it for publication was Bilal A. Khawaja.

To avoid these perturbations, it is necessary to perform traffic corrections. Traditionally, they were managed by train drivers, who modified train speed and platform dwell times to make up for their own delays, as well as by line controllers, who advanced or delayed train departures depending on the overall traffic conditions. However, in lines equipped with ATO systems, these corrections can be automated.

The corrections can be classified into two levels. On the one hand, when a disruption is too severe, it becomes impossible to maintain or return to the nominal timetable. For such cases, various methods have been developed to generate a new schedule and thus minimize the impact of the disruption on service quality [5], [6]. Nowadays, rescheduling decisions are made by operators, whose actions may be supported by computational methods such as those mentioned above.

On the other hand, it is essential to have an Automatic Train Regulation (ATR) layer when the disturbances on the line are moderate enough to allow the system to maintain or return to the nominal schedule and headway. The ATR involves generating regulation commands to trains, indicating adjustments to running and dwell times in order to meet the current traffic needs. If the line is not equipped with ATR, these regulation commands are sent to the trains by operators who can be helped by decision support systems. For instance, [7] proposes an off-line model to adjust train speed profiles by implementing strategic speed limits in specific block sections and reducing spatial headways between successive trains to enhance the capacity of the line; and [8] presents a machine learning algorithm that supports operators' decision-making by predicting delay recovery through the analysis of adjustments in train dwell and running times. On the contrary, if the line is equipped with ATR systems, the sending of regulation commands to trains can be performed without human supervision.

Nowadays, ATR systems have been developed and implemented along with ATO, where ATR constantly supervises the traffic performance and sends the regulation commands to the trains to be executed by the ATO [9]. The predictive mathematical algorithm for complex line topologies proposed in this paper focuses on this level of automatic train regulation, as its objective is to send the optimal regulation commands to trains for automatic regulation before a full rescheduling of the system's operation becomes necessary.

In the literature, several algorithms have been developed to improve ATR. For instance, in [10], a distributed Adaptive Optimal Control (AOC) strategy is presented to manage large-scale mass transit networks with transfer coordination constraints, and [11] presents an approach that uses the combination of multiple AI algorithms through an averaging mechanism to adjust in real-time the dwell times, taking into account sudden passenger fluctuations.

Focusing on the technique used for the proposed approach, Model Predictive Control (MPC) has proven effective for ATR in urban mass transit lines, offering a predictive constraint-aware multivariable control. Studies show how MPC enhances urban railway performance and reliability (..) [12]. For instance, [13] presents a stability-enhanced MPC for a single train focused on optimizing speed tracking accuracy, platform stopping precision, passenger comfort, and operational safety, considering distance and relative speed between train cars and [14] proposes an off-line two-stage optimization approach to optimize the train schedule and circulation plan with consideration of passenger demand for a simple-topology urban rail transit line that can also be applied on-line by introducing the MPC framework and reducing the optimization horizon. Additionally, robust MPC variants address uncertainties in demand and disturbances, improving schedule adherence [15].

Energy-management strategies can be developed too with MPC. For instance, [16] proposes a distributed model predictive control (DMPC) strategy for energy-saving train regulation, where the optimization is performed locally to each train based on its immediate neighbors' state. In [17], an optimization of train trajectories is used to minimize energy consumption while maintaining service quality for a follow-up line with a simple topology. Reference [18] presents a predictive model focused on minimizing the substation peak power by avoiding multiple simultaneous accelerations.

Passenger comfort and flow are also considered by using an MPC to adjust operations to reduce waiting times and overcrowding while maintaining service quality [19], [20]. Some approaches, like the nonlinear mixed-integer model in [21], further refine train regulation strategies.

Recently, the advent of new technologies that enable continuous communication between trains and the control centers to regulate the traffic, such as CBTC for metro lines and ERTMS for long-distance lines, has allowed for improving the punctuality, regularity, and even the energy consumption, among others. This is because trains can receive regulation commands at any point along the line.

Several studies have presented models specifically designed to take advantage of these systems. In [22] a model based on predictive control to improve punctuality under minor disruptions is developed; in [23] a distributed model predictive control is used to handle the safety constraints for a stable dynamic coupling of virtually coupled train set to enhance the capacity of a follow-up section of a line and with respect to computational efficiency; and the work in [24] presents a recurrent neural network-based real-time operation optimization model trained using data representing the moments when the trains departed from the platforms to reduce the energy consumption and passenger waiting time.

Focusing on the complex line infrastructure for which the proposed model is designed, most of the literature studies how to organize the traffic in non-real-time. For instance, [25] presents a mathematical model and a genetic algorithm to organize the traffic in the trunk and branches of a line; [26] presents a train timetable optimization considering a line with short-turning; [27] proposes an integrated

optimization approach for commuter metro lines by combining train timetabling, passenger flow control, and short-turning schemes to improve service efficiency; and [28] introduces a service replanning model that integrates express/local and short-turning strategies using a linearized mixed-integer non-linear programming (MINLP) approach to reduce total passenger travel time and operational costs.

Furthermore, in [29] it is proposed an offline traffic organization tool for unbalanced demand scenarios consisting of an integrated optimization model for train timetabling and rolling stock circulation that incorporates flexible short-turning and energy-saving strategies; [30] proposes a MPC-based model which minimizes the energy consumption and the deviations with respect to the schedule in overtaking maneuvers at junctions or stations; and [31] presents several optimization problems to minimize operational costs and passenger waiting time by obtaining a planning performing short turning and skip-stop strategies.

Other studies have focused on developing models for virtual coupling technology. For instance, [32] presents a hierarchical control framework for virtual coupling in a short section of a line, including a single junction to find the optimal train sequence after the track convergence with decentralized local train coordination; [33] presents an offline strategic framework that optimizes train convoy compositions for virtual coupling at junctions by maximizing bottlenecks capacity; and [34] propose a RL-based MPC for the dynamic decoupling of virtually coupled trains in throat areas, optimizing spacing while ensuring safety and efficiency through adaptive parameter fine-tuning.

Finally, the short-turning strategy has been used by several projects, like the ones focused on a reduction of the utilization of trains [35], on a reduction in passengers' waiting time [36], and on a reduction of operational costs [37].

After reviewing the existing literature, a critical research gap has been identified: enabling the restoration of nominal operations after moderate disruptions when the line is not limited to a simple or looped infrastructure. Consequently, this paper presents a new centralized predictive train regulation algorithm for complex topology lines, including short turnings and bifurcations, under continuous communication as part of the Europe's Rail FP1-MOTIONAL project [38], whose key contributions to the state of the art are:

- It is proposed a centralized real-time Automatic Train Regulation (ATR) model for complex line topologies, explicitly handling bifurcations and short-turning operations under moderate disturbances. Consequently, the proposed model, taking into account passenger comfort and operation efficiency, generates optimal regulation commands on train running and dwell times to restore the nominal timetable and headway.
- A novel theoretical approach that separates control actions into positive and negative components has been implemented to achieve an energy-efficient cost function decomposition. This multi-objective optimization strategy allows for granular penalization of energy-intensive maneuvers, achieving significant efficiency gains without compromising headway regularity.
- In addition to the typical operational and signalling constraints, the proposed model includes additional restrictions to represent maneuvers at switches and short turns that can be found in complex metro topologies within the predictive horizon. This ensures that the generated control actions are technically feasible for real-world signalling systems.

A simulator of a real railway line has been developed to evaluate the performance of the proposed algorithm in comparison with conventional regulation systems. The results demonstrate that this approach effectively restores the line's scheduled timetable and nominal headway more efficiently, aligned with the specific routes each train must follow. Additionally, the algorithm achieves a significant reduction in energy consumption and the low computational delay ensures the practical applicability of the controller for closed-loop regulation in modern mass transit infrastructures.

With respect to the paper's structure, Section II presents the problem description, Section III details the traffic model, and Section IV describes the model predictive control. Finally, Sections V, VI and VII provide the case study, results and conclusions, respectively.

II. PROBLEM DESCRIPTION

A complex topology mass-transit line with one track per direction and terminal stations is considered. It is worth noting that each station is assumed to have one platform per direction, and that, for this study, a node is defined as a point where multiple tracks converge, thereby constituting a potential bottleneck.

Two types of nodes may appear. On the one hand, there is the node corresponding to the short-turning strategy, where trains can turn around before reaching the terminal station of the line. In railway operations, this maneuver consists of a train reversing its direction at a designated turnback point, so that its head and tail are effectively swapped, and the train re-enters the line in the opposite direction. This is not a geometric change of trajectory but an operational process subject to signalling, routing, and infrastructure constraints, including switch configurations, track availability, and conflict avoidance with other trains. On the other hand, there is the node corresponding to a bifurcation, which consists of a main trunk that splits into an upper branch and a lower branch.

In **Figure 1**, a diagram of the two types of nodes is shown, where the key platforms are named with capital letters, since it will be helpful in the following sections. To generalize, it has also been marked the maneuvering point (P) where trains that come from track 2 and make the intermediate turnback stop to change the run direction. Nevertheless, this point can coincide with platform C.

The terminal stations are modeled as turnback platforms. Trains travel in both directions, stopping at platforms along

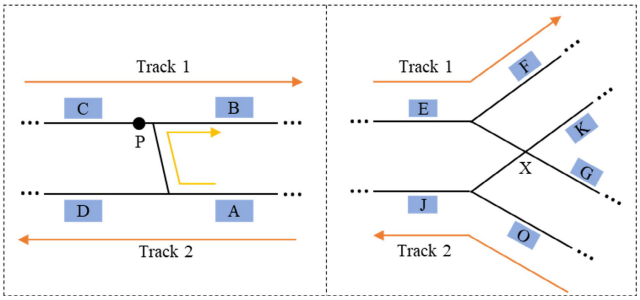

FIGURE 1. Short turning (left side) and bifurcation (right side) nodes.

the route, each of which is equipped with a platform for each direction.

III. TRAFFIC MODEL

As previously described, the traffic system is represented as a set of N trains ($i = 1$ to N) operating along M platforms ($k = 1$ to M), where each train i follows train $i-1$ and performs scheduled stops at platforms to allow passengers to get on and off.

In addition, the following assumptions are considered:

- Train overtaking is not allowed.
- Station skipping is not considered (no skip-stop operations).
- Each train has a predefined route that cannot be modified by the model.

Previous assumptions are considered because the model aims to manage moderate disturbances that do not require major rescheduling, such as traffic reordering or rerouting.

The essential variables in the model are described in Table 1.

Given a scheduled departure and arrival time (Td_k^i and Ta_k^i respectively) for train i to platform k, the corresponding nominal dwell time S_{0k} at that platform is computed as:

$$S_{0k} = \mathrm{Td}_k^i - \mathrm{Ta}_k^i \tag{1}$$

Under nominal operating conditions, a nominal headway H is maintained between successive trains, such that train i follows train i−1. This nominal headway is defined as:

$$H = Td_k^i - Td_k^{i-1} \tag{2}$$

The nominal running time R_k between platform k and platform k + 1 is calculated as follows:

$$R_k = \mathrm{Ta}_{k+1}^i - \mathrm{Td}_k^i \tag{3}$$

At both the departure and arrival times of a train at a given platform, the actual (measured) times are denoted by td_k^i and ta_k^i, respectively. The corresponding measured headway h_k^i for train i at the departure from platform k is defined as:

$$h_k^i = \mathrm{td}_k^i - \mathrm{td}_k^{i-1} \tag{4}$$

Thus, it can be defined the deviation from the scheduled departure time Xd_k^i of train i at platform k and the deviation from the scheduled arrival time Xa_k^i of train i at platform k, shown in (5) and (6), respectively

$$\mathrm{Xd}_k^i = \mathrm{td}_k^i - \mathrm{Td}_k^i \tag{5}$$

TABLE 1. Variables description.

Notation	Description
α_k	Proportional constant involved in the extra dwell time at platform k due to delays.
a_{pos}	Positive weighting factor of running-time control action.
a_{neg}	Negative weighting factor of the running-time control action.
b^i	Non-decision variable that indicates whether each train i takes the upper branch or not at the bifurcation node.
b_{pos}	Positive weighting factor of dwell-time control action.
b_{neg}	Negative weighting factor of dwell-time control action.
c	Weighting factor of the slack variable.
d^i	Non-decision variable that indicates whether train i takes the diverging route at the short-turn switch or not.
H	Nominal headway between consecutive trains.
h_k^i	Measured headway of train i at departure from platform k.
I	Minimum headway between consecutive trains.
I_{mink}	Minimum headway at platform k arrival.
L	Number of platforms in the optimization horizon.
M	Number of platforms.
N	Number of trains.
p	Weighting factor of timetable deviation.
q	Weighting factor of headway deviation.
R_k	Nominal travel time between platform k and platform $k+1$.
S_{0k}	Nominal dwell time at platform k.
s_k^i	Dwell time of train i at platform k.
sg_k^i	Positive slack variable that allows long running times for the train i from platform k to $k+1$.
t	Actual train time.
Ta_k^i	Nominal arrival time of train i at platform k.
ta_k^i	Actual arrival time of train i at platform k.
Td_k^i	Nominal departure time of train i at platform k.
td_k^i	Actual departure time of train i at platform k.
to_k	Objective running time from platform k to platform $k+1$.
up_k^i	Control action that modifies the nominal dwell time of train i at platform k.
UPmax_k	Control action that adds the maximum comfortable time to the dwell time between the platform k and $k+1$.
UPmin_k	Control action that adds the minimum comfortable time to the dwell time at platform k.
upneg_k^i	Negative control action that modifies the nominal dwell time of train i at platform k.
uppos_k^i	Positive control action that modifies the nominal dwell time of train i at platform k.
ur_k^i	Control action that modifies the nominal running time of train i from platform k to platform $k+1$.
URmax_k	Control action that adds the maximum comfortable time to the running time between the platform k and $k+1$.

TABLE 1. *(Continued.)* **Variables description.**

URmin_k	Control action that adds the minimum comfortable time to the running time between the platform k and $k+1$.
urneg_k^i	Negative control action that modifies the nominal running time of train i from platform k to platform $k+1$.
urpos_k^i	Positive control action that modifies the nominal running time of train i from platform k to platform $k+1$.
X^i	Current delay of train i.
Xa_k^i	Deviation from the scheduled arrival time of train i at platform k.
Xd_k^i	Deviation from the scheduled departure time of train i at platform k.
Y_k^i	Deviation from the nominal headway for train i measured at platform k departure.

$$\text{Xa}_k^i = \text{ta}_k^i - \text{Ta}_k^i \tag{6}$$

Additionally, the deviation from the nominal headway, denoted by Y_k^i, for train i at the departure from platform k is calculated as the difference between the actual measured headway and the nominal headway, which can be expressed as:

$$Y_k^i = \text{Xd}_k^i - \text{Xd}_k^{i-1} \tag{7}$$

The signalling system is integrated into the traffic model by the minimum headway constraints. The arrival time of train i at platform k is constrained by the departure time of the preceding train i − 1 from the same platform, according to the following inequality:

$$\text{ta}_k^i - \text{td}_k^{i-1} \geq I_{mink} \tag{8}$$

where I_{mink} represents the minimum headway at the arrival to platform k

By subtracting () and (4) from (8), the minimum headway constraint is obtained:

$$\text{Xa}_k^i - \text{Xd}_k^{i-1} \geq I_{mink} + S_{0k} - H_n \tag{9}$$

Moreover, it is necessary to include the minimum headway constraints that apply at each type of node in the complex topology to take into account the restrictions imposed by the maneuvers.

First, the minimum headway constraints in the short-turning node are analyzed. On the left side of **Figure 1**, the platforms involved in these constraints are referenced.

In this node, some trains run in the straight direction from A to D and from C to B. Other trains perform the turn-back maneuver in which the train running from platform A reaches the maneuvering point P taking the divergent route in the switch. Then it stops at that point, the time needed to move the switch (that also includes the time to dissolve the previous route and establish the new one) and the inversion time (needed to change the direction of the run). Finally, a second movement is performed from the maneuvering point P to the platform B.

The following constraints are identified in this maneuver to be added to the traffic model.

- Minimum headway between the departure of train $i-1$ from platform B and the departure of train i from platform P.

$$I_{BP} - H_{BP} \leq \text{Xd}_P^i - \text{Xd}_B^{i-1} \tag{10}$$

where H_{BP} represents the scheduled headway between the departure of the train $i-1$ from platform B and the departure of train i from point P ($H_{BP} = \text{Td}_P^i - \text{Td}_B^{i-1}$), and I_{BP} is the minimum headway between the departure of a train $i-1$ from platform B and the departure of another train i from platform P ($I_{BP} \leq \text{td}_P^i - \text{td}_B^{i-1}$).

- Minimum headway between the departure of a train from A to take the diverted track and the departure of the posterior train from A to take the main track.

$$I_1 - H_1 \leq \text{Xd}_A^i - \text{Xd}_A^{i-1} + M\left(1 - \left(1 - d^i\right) d^{i-1}\right) \tag{11}$$

where H_1 represents the scheduled headway between the departure of the train $i-1$ from platform A to take the diverted track and the departure of train i from platform A to take the main track ($H_1 = \text{Td}_A^i - \text{Td}_A^{i-1}$), and I_{BP} is the minimum headway between the departure of a train $i-1$ from platform A to take the diverted track and the departure of train i from platform A to take the main track ($I_1 \leq \text{td}_A^i - \text{td}_A^{i-1}$). M is a constant with a very big value compared with the rest of the variables and d^i is a predefined-non-decision variable that indicates whether train i takes the diverging route at A ($d^i = 1$) or not ($d^i = 0$).

- Minimum headway between the departure of a train from A to take the main track and the departure of the posterior train from A to take the diverted track.

$$I_2 - H_2 \leq \text{Xd}_A^{i-1} - \text{Xd}_A^i + M(1 - \left(1 - d^{i-1}\right) d^i) \tag{12}$$

where H_2 represents the scheduled headway between the departure of the train $i-1$ from platform A to take the main track and the departure of train i from platform A to take the diverted track ($H_2 = \text{Td}_A^i - \text{Td}_A^{i-1}$), and I_{BP} is the minimum headway between the departure of a train $i-1$ from platform A to take the main track and the departure of train i from platform A to take the diverted track ($I_2 \leq \text{td}_A^i - \text{td}_A^{i-1}$).

- Minimum headway between the departure of a train from P and the departure of the posterior train from A to take the diverted track.

$$I_{PA} - H_{PA} \leq \text{Xd}_A^i - \text{Xd}_P^j + M(1 - d^i) \tag{13}$$

where j is the same train as $i - (r^{-1} - 1)$ and r is the ratio of trains that perform a short-turning operation. For instance, if $r = 1/2$, every second train turns around. H_{PA} represents the scheduled headway between the departure of the train j from P and the departure of

train i from platform A to take the diverted track ($H_{PA} = \mathrm{Td}_A^i - \mathrm{Td}_P^j$), and I_{PA} is the minimum headway between the departure of a train j from P and the departure of train i from platform A to take the diverted track ($I_{PA} \leq \mathrm{td}_A^i - \mathrm{td}_P^j$).

- Minimum headway between the departure of a train from P and the departure of the posterior train from C.

$$I_P - H_P \leq \mathrm{Xd}_C^i - \mathrm{Xd}_P^{i-1} \tag{14}$$

where H_P represents the scheduled headway between the departure of the train $i-1$ from P to and the departure of train i from platform C ($H_P = \mathrm{Td}_P^i - \mathrm{Td}_P^{i-1}$), and I_P is the minimum headway between the departure of a train $i-1$ from P to take and the departure of train i from platform C ($I_2 \leq \mathrm{td}_A^i - \mathrm{td}_A^{i-1}$).

Once the minimum headway constraints to be added to the traffic model due to the short-turning node have been explained, the minimum headway constraints to be incorporated due to the presence of a bifurcation node are presented. It is recalled that the right side of **Figure 1** shows a bifurcation node with the representative platforms, so the platforms involved in these equations are referenced to those ones.

To these new equations, the predefined-non-decision variable b^i indicates whether each train takes the upper branch ($b^i = 1$) or not ($b^i = 0$).

- Minimum headway between the departure of train $i-1$ from platform E to take the upper branch and the departure of train i from platform E to take the lower branch.

$$I_{1Y} - H_{1Y} \leq \mathrm{Xd}_E^i - \mathrm{Xd}_E^{i-1} + M(1 - \left(1 - b^i\right) b^{i-1}) \tag{15}$$

where H_{1Y} represents the scheduled headway between the departure of the train $i-1$ from platform E to take the upper branch and the departure of train i from platform E to take the lower branch ($H_{1\_Y} = \mathrm{Td}_E^i - \mathrm{Td}_E^{i-1}$), and I_{1Y} is the minimum headway between the departure of a train $i-1$ from platform E to take the upper branch and the departure of train i from platform E to take the lower branch ($I_{1Y} \leq \mathrm{td}_E^i - \mathrm{td}_E^{i-1}$).

- Minimum headway between the departure of train $i-1$ from platform E to take the lower branch and the departure of train i from platform E to take the upper branch.

$$I_{2Y} - H_{2Y} \leq \mathrm{Xd}_E^i - \mathrm{Xd}_E^{i-1} + M(1 - \left(1 - d^{i-1}\right) d^i) \tag{16}$$

where H_{2Y} represents the scheduled headway between the departure of the train $i-1$ from platform E to take the lower branch and the departure of train i from platform E to take the upper branch ($H_{2Y} = \mathrm{Td}_E^i - \mathrm{Td}_E^{i-1}$), and I_{2Y} is the minimum headway between the departure of a train $i-1$ from platform E to take the lower branch and the departure of train i from platform E to take the upper branch ($I_{1Y} \leq \mathrm{td}_E^i - \mathrm{td}_E^{i-1}$).

- Minimum headway between the departure of train $i-1$ from platform O and the departure of a train i from K.

$$I_{OK} - H_{OK} \leq \mathrm{Xd}_K^i - \mathrm{Xd}_O^{i-1} \tag{17}$$

where H_{OK} represents the scheduled headway between the departure of the train $i-1$ from platform O and the departure of train i from platform K ($H_{OK} = \mathrm{Td}_K^i - \mathrm{Td}_O^{i-1}$), and I_{OK} is the minimum headway between the departure of a train $i-1$ from platform O and the departure of train i from platform K ($I_{OK} \leq \mathrm{td}_K^i - \mathrm{td}_O^{i-1}$).

- Minimum headway between the departure of train $i-1$ from platform K and the departure of a train i from O.

$$I_{OK} - H_{OK} \leq \mathrm{Xd}_K^i - \mathrm{Xd}_O^{i-1} \tag{18}$$

where H_{KO} represents the scheduled headway between the departure of the train $i-1$ from platform K and the departure of train i from platform O ($H_{KO} = \mathrm{Td}_O^i - \mathrm{Td}_K^{i-1}$), and I_{KO} is the minimum headway between the departure of a train $i-1$ from platform K and the departure of train i from platform O ($I_{KO} \leq \mathrm{td}_O^i - \mathrm{td}_K^{i-1}$).

- Minimum headway between the departure of train i from platform K towards J and the departure of a train j from platform E to take the lower branch.

$$I_{KE} - H_{kE} \leq \mathrm{Xd}_E^j - \mathrm{Xd}_K^i + M \cdot b^j \tag{19}$$

where j is the train that will pass through the crossing X after the train i that departed from K passed through that point. H_{KE} represents the scheduled headway between the departure of the train i from platform K and the departure of train j from platform E to take the lower branch ($H_{KE} = \mathrm{Td}_E^j - \mathrm{Td}_K^i$), and I_{KE} is the minimum headway between the departure of a train i from platform K and the departure of train j from platform E to take the lower branch ($I_{KE} \leq \mathrm{td}_E^j - \mathrm{td}_K^i$).

- Minimum headway between the departure of train i from platform E to take the lower branch and the departure of a train j from K in the opposite direction towards J.

$$I_{EK} - H_{EK} \leq \mathrm{Xd}_K^j - \mathrm{Xd}_E^i + M \cdot b^i \tag{20}$$

where j is the train that will depart from K after train i has passed through the crossing X in **Figure 1**.

Additionally, H_{EK} represents the scheduled headway between the departure of the train j from platform E to take the lower branch and the departure of train i from platform K ($H_{EK} = \mathrm{Td}_E^i - \mathrm{Td}_K^j$), and I_{EK} is the minimum headway between the departure of a train j from platform E to take the upper branch and the departure of train i from platform K ($I_{EK} \leq \mathrm{td}_E^i - \mathrm{td}_K^j$).

After defining the minimum headway constraints, which constitute the signalling system, the running time and dwell time expressions are presented.

Variable ur_k^i denotes the control action applied to train i to modify its nominal running time from platform k to k + 1 *and*

can be expressed as:

$$\mathrm{Xa}^i_{k+1} - \mathrm{Xd}^i_k = \mathrm{ur}^i_k \tag{21}$$

Additionally, the control actions are subject to bounds, expressed as:

$$\mathrm{URmin}_k \leq \mathrm{ur}^i_k \leq \mathrm{URmax}_k \tag{22}$$

It is worth noting that speed constraints are defined during the infrastructure design stage, including both interstation segments and nodes such as bifurcations and short-turning points. These constraints determine the minimum feasible running time (urmin^i_k), which is used as an input parameter in the model. In addition, speed limits are inherently reflected in the signalling constraints governing safe train operations. For interstations associated with diverging routes (bifurcations and short-turning nodes), the lower bounds of the running-time control actions are set to zero. This reflects the reduced operational flexibility in these sections, where low speeds required by the maneuver prevent further reduction of running times.

Finally, the dwell time at platforms is modeled as a linear function of the arrival–departure headway, based on the premise that the time required for passenger boarding and alighting increases with this headway, as considered in several studies [39], [40]. Accordingly, the deviation between the departure and the arrival of a train i at a platform k depends on the dwell-time control action up^i_k (positive if the train is held at the platform and if the dwell time is reduced), and an additional dwell delay Xs^i_k caused by passenger accumulation:

$$\mathrm{Xd}^i_k - \mathrm{Xa}^i_k = \mathrm{Xs}^i_k + \mathrm{up}^i_k \tag{23}$$

where $Xs^i_k = \alpha(\mathrm{Xa}^i_k - \mathrm{Xd}^{i-1}_k)$ being α_k a proportionality constant.

Moreover, the control action is constrained within predefined bounds, similarly to the control action ur^i_k:

$$\mathrm{UPmin}_k \leq \mathrm{up}^i_k \leq \mathrm{UPmax}_k \tag{24}$$

IV. AUTOMATIC TRAIN REGULATION MODEL

The proposed automatic train regulation model is composed of two main modules, as can be seen in **Figure 2**. The first module is a mathematical predictive control algorithm that generates the running-time and dwell-time control actions (ur^i_k and up^i_k) through an optimization model, which takes into account the quantified train delays and the traffic model. The second module translates these control actions into ATO driving commands, which are then transmitted to the respective trains.

The new driving commands, resulting in new running times and dwell times, and the new position and speed of the trains are inputs of the ATR model in the next step of time to take into account the updates in the traffic.

In addition, a multi-train simulation platform based on a real mass transit line has been developed to evaluate the effectiveness of the proposed approach. This simulator incorporates a realistic ATO model, which receives the regulation commands generated by the ATR system and processes them to compute the traction force required from each train's motor.

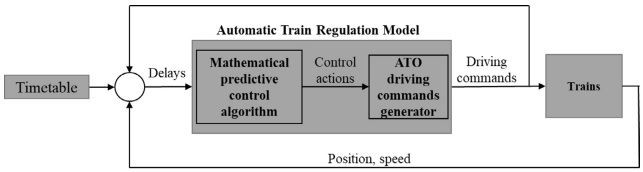

FIGURE 2. Predictive automatic train regulation model structure.

A. MATHEMATICAL PREDICTIVE CONTROL MODEL

The mathematical predictive control algorithm (see **Figure 2**) calculates the running time and dwell time control actions (ur^i_k and up^i_k respectively) by quantifying train delays through a convex quadratic programming optimization framework that will be solved using constrained least squares. It is recalled that the resulting control actions consist of time corrections to the nominal running and dwell times at each platform.

It is recalled that the model addresses real-time train regulation under moderate disturbances and, as detailed in the assumptions, with fixed routes, no overtaking and no skip-stop operations.

To achieve this, the primary objective is to minimize deviations from the scheduled timetable and headways over a defined prediction horizon, which corresponds to the next L platforms for each train.

1) FORMULATION OF THE MATHEMATICAL PREDICTIVE CONTROL MODEL

The Automatic Train Protection (ATP) system, which is the system responsible for enforcing safety constraints, has been considered by including a non-negative slack variable sg^i_k that permits extended running times when braking is required to avoid ATP intervention because of the proximity to another train. Consequently:

$$\mathrm{Xa}^i_{k+1} - \mathrm{Xd}^i_k = \mathrm{ur}^i_k + \mathrm{sg}^i_k \tag{25}$$

This model leverages the continuous communication capabilities provided by continuous communication systems to enable real-time ATR based on current traffic conditions. Consequently, the control actions can be generated at any moment along the train's journey, so the optimization process can be initiated even while a train is running between platforms. To accommodate this scenario, the model substitutes the standard platform-based delay term Xd^i_k with the current delay X^i for the initial platform of the simulation horizon, denoted by k_{0i}. In this case, (25) would be substituted by (26).

$$\mathrm{Xa}^i_{k_{0i}+1} - X^i = \mathrm{ur}^i_{k_{0i}} + \mathrm{sg}^i_k \tag{26}$$

For these trains, it is necessary to update the control bounds $\mathrm{URmin}_{k_{0i}}$ and $\mathrm{URmax}_{k_{0i}}$, since their ability to gain or lose time while running between platforms is more limited than

at departures. To compute these bounds, simulations are run from the current space-speed state. One uses the fastest allowable speed profile to find the minimum running time; the other uses the slowest comfortable speed to find the maximum. The bounds are the differences from the nominal running time.

Consequently, for this case, (22) will be replaced by (27):

$$\mathrm{URmin}_{k_{0i}} \leq \mathrm{ur}^i_{k_{0i}} \leq \mathrm{URmax}_{k_{0i}} \tag{27}$$

Following the same reasoning, the optimization process can be initiated when a train is stopped at a platform. In this case, the bounds for the dwell-time control action UPmin_k and UPmax_k must be updated at the first platform k_{0i} within the optimization horizon:

$$\mathrm{UPmin}_{k_{0i}} = \max\left[\mathrm{UPmin}_k, T - \left(\mathrm{Ta}^i_k + S_{0k} + \mathrm{Xs}^i_k\right)\right] \tag{28}$$

$$\mathrm{UPmax}_{k_{0i}} = \max\left[\mathrm{UPmax_k}, T - \left(\mathrm{Ta}^i_k + S_{0k} + \mathrm{Xs}^i_k\right)\right] \tag{29}$$

As a result, (24) is replaced by (30) when $k = k_{0i}$:

$$\mathrm{UPmin}_{k_{0i}} \leq \mathrm{up}^i_{k_{0i}} \leq \mathrm{UPmax}_{k_{0i}} \tag{30}$$

It is important to note that the control actions up^i_k and ur^i_k directly impact the train's energy consumption. Shorter running times ($\mathrm{ur}^i_k < 0$) lead to higher energy usage, whereas longer running times ($\mathrm{ur}^i_k > 0$) result in lower energy consumption.

Therefore, the decomposition of the control actions into their positive and negative components (urpos^i_k, urneg^i_k, uppos^i_k and upneg^i_k) allows the formulation of an optimization problem with a cost function that not only accounts for ATR objectives and passenger comfort but also incorporates energy efficiency considerations. For instance, giving more weight to negative running time control actions penalizes shorter running times that are the most energy-consuming ones. Besides, by penalizing larger dwell times, the model compensates by increasing running times, producing a lower energy consumption.

Consequently, the control actions can be expressed as follows:

$$\mathrm{ur}^i_k = \mathrm{urpos}^i_k - \mathrm{urneg}^i_k \tag{31}$$

$$\mathrm{ur}^i_{k_{0i}} = \mathrm{urpos}^i_{k_{0i}} - \mathrm{urneg}^i_{k_{0i}} \tag{32}$$

$$\mathrm{up}^i_k = \mathrm{uppos}^i_k - \mathrm{upneg}^i_k \tag{33}$$

$$\mathrm{up}^i_{k_{0i}} = \mathrm{uppos}^i_{k_{0i}} - \mathrm{upneg}^i_{k_{0i}} \tag{34}$$

where

$$\{\mathrm{urpos}^i_k, \mathrm{urneg}^i_k, \mathrm{urpos}^i_{k_{0i}}, \mathrm{urneg}^i_{k_{0i}}, \mathrm{uppos}^i_k, \mathrm{upneg}^i_k, \mathrm{uppos}^i_{k_{0i}}, \mathrm{upneg}^i_{k_{0i}}\} \geq 0 \tag{35}$$

A prediction horizon is established, comprising the following L platforms for which the arrival and departure delays of each train (Xa^i_k and Xd^i_k) are determined, as well as the travel and stop control actions at each platform (ur^i_k and up^i_k) and the slack variable sg^i_k.

The cost function that minimizes regularity criteria during the prediction horizon and the magnitude of control actions and slack variables, taking into account energy efficiency criteria, is defined as:

$$\begin{aligned} J = {} & p\sum_{i,k}\left(\mathrm{Xd}^i_k\right)^2 + q\sum_{i,k}\left(\mathrm{Xd}^i_k - \mathrm{Xd}^{i-1}_k\right)^2 \\ & + a_{pos}\sum_{i,k}\left(\mathrm{urpos}^i_k\right)^2 + a_{neg}\sum_{i,k}\left(\mathrm{urneg}^i_k\right)^2 \\ & + b_{pos}\sum_{i,k}\left(\mathrm{uppos}^i_k\right)^2 + b_{neg}\sum_{i,k}\left(\mathrm{upneg}^i_k\right)^2 \\ & + c\sum_{i,k}\left(\mathrm{sg}^i_k\right)^2 \end{aligned} \tag{36}$$

For each train i, with $i : 1 \leq i \leq N$, and for each platform k, where $k : k_{0i} \leq k \leq k_{0i} + L$, with k_{0i} being the next departure platform of train i and L denoting the number of platforms in the prediction horizon.

The first and second term stands for the deviation with respect to the nominal schedule and nominal headway respectively; the third and fourth term stands for the positive and negative running-time control actions emitted, respectively; the fifth and sixth term stands for the positive and negative dwell-time control actions emitted; and, finally, the seventh term stands for the non-negative slack variable sg^i_k that permits extended running times when braking is required to avoid ATP intervention.

Additionally, constants p and q are used to weight the deviation from the nominal schedule and from the nominal headway, respectively. Similarly, constants $a_{pos}, a_{neg}, b_{pos}$ and b_{neg} serve to weight the positive and negative control actions for the running time and dwell time. Lastly, constants c and d represents the weight of the slack variables, and it is set high enough to ensure minimal intervention from the signalling systems.

The initial conditions of the optimization problem are determined by each train's position along the line and its current delay. For each train, two scenarios are distinguished:

If the train is stopped at a platform. The deviation from the scheduled arrival time $\mathrm{Xa}^i_{k_0}$ at the first platform k_0 must be established as

$$\mathrm{Xa}^i_{k_0} = \mathrm{Xa}^i_k \tag{37}$$

If the train is currently travelling between platforms: the current delay X^i relative to the nominal schedule at the train's current position must be defined as

$$X^i = \mathrm{Xd}^i_{k_0} + \Delta X \tag{38}$$

where $\mathrm{Xd}^i_{k_0}$ represents the departure delay of train i from the last platform k_0, and ΔX represents the difference in running time between the actual train movement and the nominal movement from the last departure to the current train position.

A positive ΔX indicates an increased delay since the last departure, whereas a negative ΔX stands for delay recovery.

In lines equipped with continuous communication systems, it's possible to determine delays X^i at any point along the train's current position. This capability allows the ATR system to immediately update control commands whenever a delay occurs, improving how these disruptions are managed. On the other hand, in lines that use signalling systems based on discrete communications, these delays are only updated and corrected when the train is at the platforms.

2) RESOLUTION OF THE OPTIMIZATION PROBLEM

The convex quadratic optimization control problem is defined by its cost function described in (36); the initial conditions defined in (37) or (38) depending on each train initial state; the traffic model constraints for $k > k_{0i}$ outlined in (8), (21), (22), (23), (24), (25), (31), (33), (35); the traffic model constraints for $k = k_{0i}$ outlined in (26), (27), (30), (32), (34); the minimum headway constraints due to the short-turning node outlined in (10), (11), (12), (13), (14); and the minimum headway constraints due to the bifurcation node outlined in (15), (16), (17), (18), (19), (20) of which (19) and (20) can be removed if the node is equipped with a flyover, since in that situation the X-crossing in **Figure 1** would no longer be a conflict point. The constraints of the nodes will be applied as many times as there are nodes of each type in the topology.

The optimization problem calculates the running-time and dwell-time control actions for each platform in the horizon simulation L. Nevertheless, each train will receive the running-time and dwell-time control actions corresponding to the first interstation of that simulation horizon L.

The optimization model is run at regular time intervals (the control cycle) to determine the next control commands for the dwell time up_k^i and for the running time ur_k^i.

B. ATO DRIVING COMMANDS GENERATOR

This subsection addresses the second module (**Figure 2**) of the proposed ATR model, which translates the control actions calculated by the mathematical predictive control algorithm into specific driving commands to be sent to each train.

The traffic regulation model is designed around continuous communication, allowing for constant regulation since trains can receive control commands at any point along the route. This approach improves operational efficiency and enhances the system's responsiveness to any disruptions.

It is worth noting that the algorithm has been designed to handle lines with complex topology, including scenarios like short-turning strategies or bifurcation nodes, so it is ensured that the control actions and corresponding driving commands remain valid and accurate even in lines where not all trains follow the same route.

The running-time control actions calculated by the mathematical predictive control algorithm are used to compute the Automatic Train Operation (ATO) driving commands for the trains. The traditional ATO systems implemented in mass transit lines for decades use driving commands based on either maintaining a constant target speed set by the speed regulation command v_{reg} or operating in coasting-remotoring cycles controlled by the coasting speed v_d and the remotoring speed v_r [41]. These driving commands define the speed profile to be performed by the train.

However, in new ATO developments, such as the standard to work with ERTMS (European Rail Traffic Management System), the driving commands are arrival, departure or passing times at specific locations (Timing Points). Then, the ATO on board equipment is responsible for calculating a speed profile to adhere to the received Timing Points.

The ATR model proposed in this paper can be applied to both systems. In the case of traditional ATO systems, the proposed model only needs to include a layer to calculate the speed-based commands after obtaining the target arrival/departure time.

This paper presents the application to traditional ATO systems where the driving commands generator modifies v_{reg} or v_d and v_r to achieve different interstation running times.

When a train departs from a platform, the desired travel time to the next platform is computed:

$$\mathrm{to}_{k_{0i}} = R_{k_{0i}} + \mathrm{ur}^i_{k_{0i}} \tag{39}$$

where $\mathrm{to}_{k_{0i}}$ is the target running time for train i from the initial platform k_{0i} to platform $k_{0i}+1$, $R_{k_{0i}}$ is the nominal running time from the schedule, and $\mathrm{ur}^i_{k_{0i}}$ is the correction for the running time calculated by the predictive control algorithm in its latest execution.

Once the target running time is calculated, thanks to the high bandwidth, a speed profile will be chosen from a Pareto front, ensuring that for every possible travel time there is a corresponding profile that minimizes energy consumption while also respecting comfort requirements [42]. This speed profile sets the ATO driving commands.

On the other hand, if the train is running an interstation, the target time $\mathrm{to}_{k_{0i}}$ from the current position of the train pos to the next platform is calculated in every regulation cycle as:

$$\mathrm{to}_{k_{0i}} = R^{pos}_{k_{0i}} + \mathrm{ur}^i_{k_{0i}} \tag{40}$$

where $R^{pos}_{k_{0i}}$ is the nominal running time from the train's current position to the next platform.

If the train is in traction, both v_r and v_d will be reduced by the same velocity increment until a minimum remotoring velocity or until the target time is met. If the minimum remotoring velocity is reached, it is possible to reduce the coasting velocity until a minimum difference between v_d and v_r.

If the train is coasting, only the remotoring velocity will be reduced until the target time is met or until the minimum remotoring velocity is reached.

V. CASE STUDY

The proposed algorithm has been validated in scenarios where trains run in a mass transit line with a complex topology.

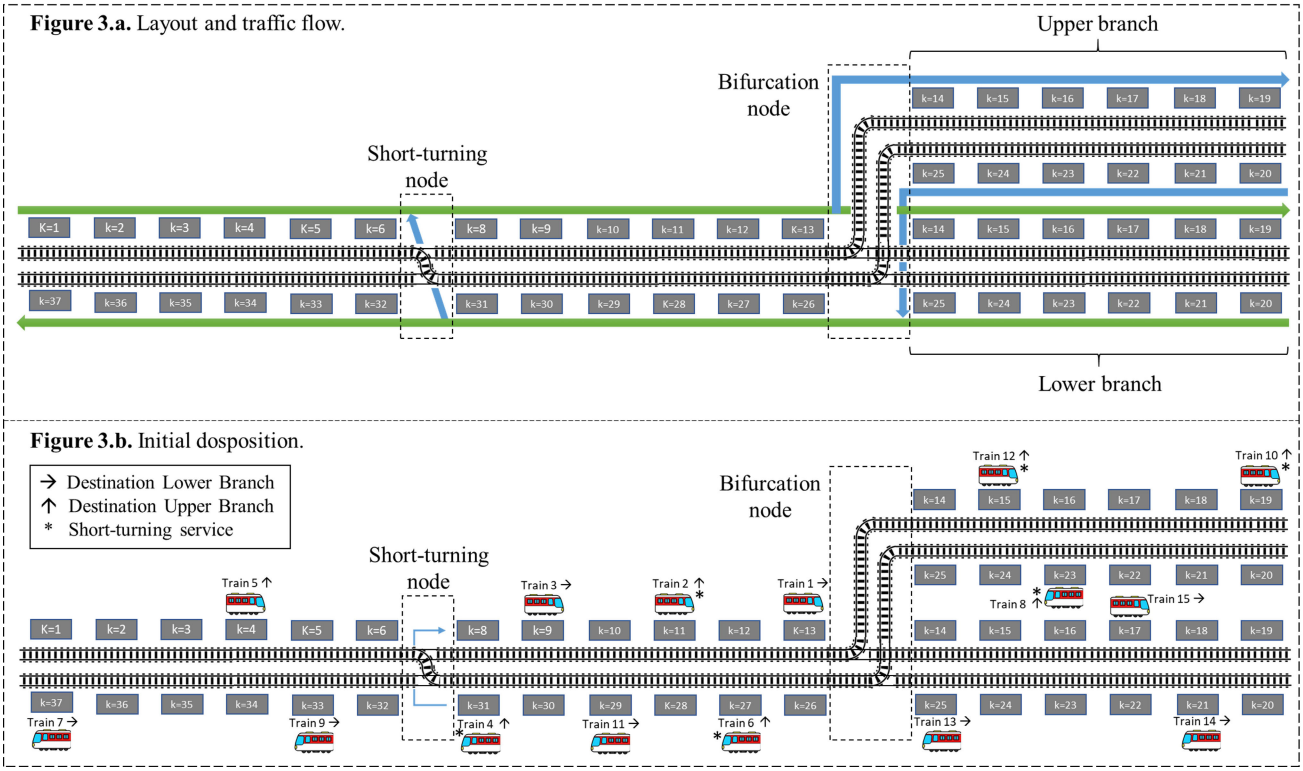

FIGURE 3. Layout, traffic flow and initial disposition.

Figure 3 illustrates both the track topology and the corresponding train operation considered in this case study. For clarity, the figure is divided into two parts. On the one hand (Figure 3.a), the infrastructure layout is presented, **3** including the main line, a bifurcation node without a flyover, and an intermediate turnback located between platforms $k = 6$ and $k = 7$. This turnback allows selected trains to reverse direction and re-enter the main line. The traffic flows are also represented through green (straight route) and blue (diverged route) arrows.

On the other hand (Figure 3.b), it is shown the initial distribution of trains and their assigned routes. Trains are labeled according to their destination: those assigned to the upper branch are indicated with an upward arrow, while those continuing towards the lower branch are represented with a rightward arrow, as detailed in the legend. In addition, trains marked with an asterisk (*) correspond to services performing short-turning operations at the intermediate turnback.

At the bifurcation node, trains sharing the same track segment interact before being routed towards different branches. Similarly, at the intermediate turnback, selected trains reverse their direction without completing the full route. In this scenario, a regular routing pattern is considered, where every second train is assigned to the diverging route at both the bifurcation and the turnback.

Sequential maneuvers in these nodes are implicitly enforced through signalling and operational constraints, ensuring conflict-free and temporally consistent train movements at bifurcations and short turns. The ATP-based slack variable (sg_k^i) further guarantees safe interactions.

These operational features generate interacting traffic flows with heterogeneous routes over shared infrastructure, significantly increasing the complexity of the regulation problem and providing a representative scenario to evaluate the performance of the proposed algorithm. Besides, it is recalled that, as the model proposes a centralized real-time ATR framework, all trains can receive regulation commands at any time along the journey.

Finally, to validate the algorithm and prove its robustness, it has been implemented in a simulator that replicates the operation of a real complex topology Spanish mass-transit line. This simulator (see **Figure 2**) models simultaneously 15 identical trains and calculates in every simulation step every train position, velocity, and time.

To achieve this, the simulator takes into account train dynamics, which are implemented through a physics-based train model developed in this work is described in [41]. The model depends on the traction force, running resistance, and track gradient.

The ATO takes into account the control logic to accelerate and brake for maximum speed reduction and station

approach, ensuring jerk limits for passengers' comfort. Finally, the ATP implemented takes into account the braking due to the proximity to another train.

Additionally, passenger boarding and alighting delays are simulated using lognormally distributed extra dwell times, providing a realistic representation of operational variability.

The implementation of a real-based simulator enables a detailed analysis of the algorithm's behavior under dynamic conditions, ensuring that the proposed approach can effectively manage multi-train circulation and ensure a reliable passenger service.

A. SCENARIOS CONSIDERED

For the evaluation of the proposed algorithm, three different scenarios have been considered, each progressively increasing in complexity and realism to assess the algorithm's performance under a variety of operational conditions:

Synthetic open-loop scenario. Here, the algorithm is tested in an open-loop setup, meaning it is not yet connected to the simulator and only its traffic forecast is analyzed. This configuration is particularly valuable for a detailed explanation of the algorithm's results since the algorithm's outputs can be analyzed in isolation. An initial delay is imposed on one of the trains, and the evolution of the traffic over the simulation horizon is studied. To facilitate the interpretation of the results and the discussion of the system's behavior, the algorithm considers a synthetic railway line where all the interstations have the same length and nominal running time. The maximum and minimum limits of the dwell and running-time control actions are the same across the entire prediction horizon.

Synthetic closed-loop scenario. Here, the algorithm is implemented within the simulator that models the same synthetic railway line, and only a single train experiences an initial delay, with no additional disturbances affecting the other trains or the dwell times at platforms. The purpose of this scenario is to study the transient behavior of the convoy as it recovers from this single delay. The simulator models a complex-topology mass transit line, where all interstation distances are identical, and the same control actions limits (buffers) are applied throughout the network. This uniformity makes it easier to understand and interpret the convoy's recovery dynamics.

Realistic closed-loop scenario. Here, the simulator is based on the real data of a Spanish mass transit line. In this line, all the running times and control action limits are different for each interstation because they are conditioned by variable distance between platforms, grades and speed limits. This scenario aims to evaluate the traffic evolution under normal operating conditions, accounting for realistic dwell time variations driven by stochastic passenger behavior, which introduces natural perturbations at the stops. Here, the algorithm's adaptability and robustness are tested in a more demanding and realistic environment, providing valuable insights into its effectiveness for real-world deployment.

B. TESTING PHILOSOPHY

In the second and third scenarios, the performance of three controllers is compared to demonstrate the effectiveness of the proposed algorithm in two key aspects. Firstly, the aim is to highlight the advantages of the algorithm when applied to complex mass transit lines topologies equipped with continuous communication and high bandwidth (which allows the use of the generated Pareto curve described in Section III.B.1). Secondly, the evaluation focuses on the energy-saving benefits of the algorithm, which leverages the separation of positive and negative control actions.

The three controllers considered are:

Controller (A): This controller implements the proposed predictive mathematical model to generate control actions for a line equipped with a discrete control center to train communication system. Delay tracking and control action emission occur exclusively at platform stops. Furthermore, it operates with low bandwidth, offering only four predesigned speed profiles per each interstation. In this case, the weights for positive and negative control actions in the cost function are equal.

Controller (B): This controller also implements the proposed predictive model but is designed for a line equipped with a continuous radio communication signalling system and high bandwidth, providing access to all speed profiles generated along the Pareto curve. Unlike Controller (A), delay tracking and control command emission can be performed continuously, even between platforms. As in the previous case, positive and negative control actions are weighted in the cost function with the same value.

Controller (C): This controller is identical to Controller (B) except for the configuration of the algorithm's weighting scheme. Here, the weights assigned to negative running-time control actions and positive dwell control actions are higher than those for positive running-time control actions and negative dwell control actions. This configuration aims to achieve more energy-efficient automatic train regulation.

The performance indicators for the proposed model will be determined by the objectives in the cost function: deviations from the nominal schedule, deviations from the nominal headway, and the evolution of control actions throughout the simulation scenario.

C. COMPUTATIONAL PERFORMANCE

The predictive optimization mathematical model has been implemented using the MATLAB programming language. The *lsqlin* solver is employed to solve the convex quadratic program using constrained least squares with linear constraints.

The problems have been solved using an Intel Core i7 processor with a base frequency of 2.6 GHz. The average time elapsed in generating control actions is 0.86 seconds. This time is sufficiently fast to be applied to a control cycle of 1 second, which is a typical frequency at which

continuous communication technologies recalculates train velocity profiles based on the provided control actions.

VI. RESULTS

In this section, the results of the three scenarios are presented.

A. SYNTHETIC OPEN-LOOP SCENARIO. RESULTS OF THE ALGORITHM IN OPEN-LOOP SIMULATION UNDER DIFFERENT INITIAL CONDITIONS

In this first scenario, the proposed algorithm is tested in open-loop mode, meaning it is not yet connected to the simulator, and the traffic forecast of the algorithm is analyzed facing an initial situation of train delay.

In this case, a synthetic railway line is considered where all the runs between platforms are equal. The upper limit of the running-time control action (URmax_k^i) has been set to 30 s and the lower limit (URmin_k^i) to -10 s. The upper limit of the dwell-time control action (UPmax_k^i) has been set to 20 s, and the lower limit (UPmin_k^i) to -5 s.

As discussed in Section III, negative control actions reduce dwell or running times with respect to the nominal values. Consequently, the lower bounds of these control actions must be negative. However, they must be correctly bounded to allow passengers to board the train (in the case of dwell control action) and to ensure compatibility with the fastest available interstation speed profile (in the case of running-time control action).

The schedule-related term in the objective function has been weighted with a value of $p = 0.25$, while the term related to headway quality has been weighted with $q = 1$. All running-time and dwell-time control actions (both positive and negative) have been weighted with a value of 0.1.

The weighting factors in the objective function $p = 0.25$ and $q = 1$) were selected to reflect standard operational priorities in high-frequency metro systems. During peak periods, maintaining a stable headway is typically prioritized over strict adherence to the nominal schedule to prevent train bunching and ensure uniform passenger distribution. Consequently, the weight assigned to schedule deviations has been defined as 25% of the weight for headway deviations. With respect to the control actions, the choice of applying a uniform weight of 0.1 provides a neutral baseline for the regulation strategy, ensuring that neither long nor short dwell or running times are disproportionately penalized, which allows for a clear validation of the algorithm's fundamental behavior before introducing the granular energy-efficiency discretization discussed in subsequent sections.

Finally, the prediction horizon was set to $L = 37$ steps, corresponding to a full round trip of the line. This horizon ensures the proposed model captures delay propagation across the entire topology, including all bifurcation and short-turning nodes. While shorter horizons would reduce processing time, $L = 37$ provides a comprehensive look-ahead window that guarantees traffic stability. The average computation time is 0.85 s, confirming the model's feasibility for real-time regulation.

In this initial evaluation, a deliberate initial delay is imposed on one of the trains, and the algorithm's response is studied over the simulation horizon. For easier interpretation and clearer discussion of the results, the algorithm is configured so that the maximum and minimum limits of positive and negative control actions for both running and dwell times are identical across all track sections.

To analyze the behavior of the algorithm, an initial condition has been designed in which Train 1 **(Figure 3)** is assigned a delay of 65 seconds. It is important to recall that the delays considered to test the performance of the mathematical predictive algorithm are moderate, as the objective of the proposed algorithm is to regulate train traffic in the presence of disturbances that do not require a complete traffic rescheduling.

If the delays were too large, it would be necessary to replan the traffic to ensure reliable operation.

The result for this initial condition is shown in **Figure 4**, where it is represented the delay of the trains at the moment of the departure of the platforms where those trains are going to get through, which constitutes the optimization horizon. This figure is divided between the trains that are going to take the upper and lower branches, according to **Figure 3**.

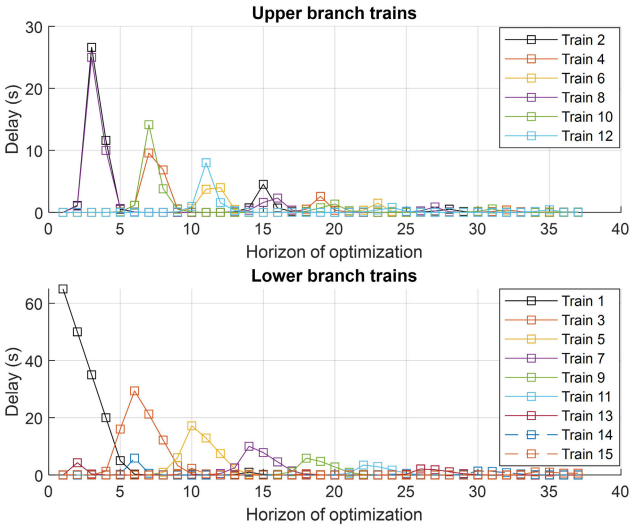

FIGURE 4. Synthetic open-loop scenario. Initial condition 1.

First, the delay of train 1 triggers a signalling delay for train 8 due to the minimum headway constraints between the passage of an ascending train and a descending train at the bifurcation node (constraint (20)) in the absence of a flyover. To regulate the headway, this delay in train 8 consequently propagates to subsequent trains operating on the upper branch, in line with their order of circulation through that branch: train 10, train 12, etc.

On the other hand, the same delay of train 1 causes an additional signalling delay in train 2, driven by the minimum headway restriction between the passage of a train through the lower branch and the next one through the upper branch

(constraint (16)). It is important to highlight that, as verified, this delay in train 2 is recovered after the train passes the switch. This is because, according to the train routes, the main perturbations are confined to the lower branch, where the significantly delayed train (train 1) is operating. Therefore, no significant delays are induced in the trains circulating along the main trunk line until reaching the platform immediately before the node, as this is the only platform in that main trunk line where the headway and schedule have not been met.

This idea is reflected in the evolution of the delays of the trains following train 2, but running along the opposite branch to train 1 (trains 4 and 6). Here, it can be observed that the delays are minimized and are precisely adjusted by the algorithm to achieve an optimal balance between maintaining their branch's schedule and correcting the headway at the last trunk line platform.

Consequently, following this same principle, the delays experienced by the trains with the same route as train 1 (trains 3, 5, 7, 9, 11, 13, 14, and 15) are more pronounced. These delays are expected to arise when the trains reach either the platform where the significant delay occurred or the preceding platform, as determined by the algorithm according to the implemented model.

Finally, a second initial condition case is proposed in which the same delay is applied to train 4, which is going to perform a mid-loop turn. **Figure 5** presents the results. In this case, the trains that will perform the short-turn are those that will go for the upper branch, according to **Figure 3**.

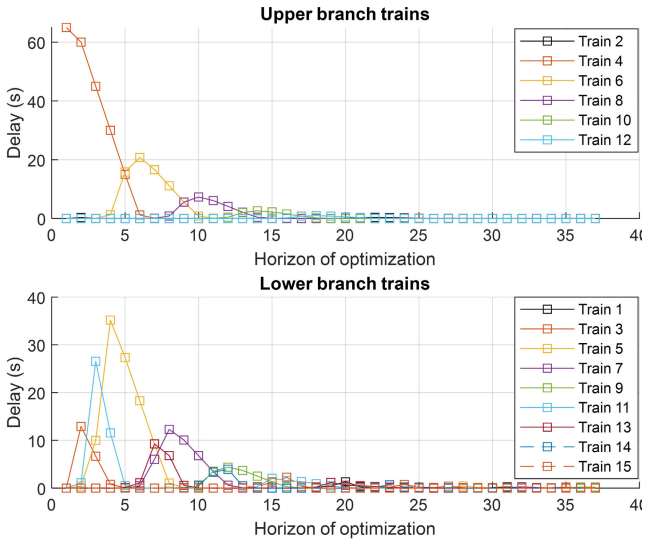

FIGURE 5. Synthetic open-loop scenario. Initial condition 2.

Similar to the previous case, the largest delays occur on the trains that are closest to the perturbed train. An initial delay is observed on train 3 to reduce the headway error because it will be ahead of train 4. Similarly, train 5 experiences a significant delay because, although it is coming from the low-demand area, it will be behind train 4, propagating this delay to all the trains that will pass through the common trunk, either because they will perform the short-turning or because they are coming from the low-density area. These trains include trains 5, 6, 7, 8, 9, and so on.

It is noted that the trains that use the common trunk but will not perform the short turning (trains 11, 13, 14) also experience delays to regulate the headway at the end of the main trunk, because the original delay was caused there. However, once they enter the low-density area, they are instructed to recover their delays as soon as possible, since this area is not affected by the perturbation.

B. SYNTHETIC CLOSED-LOOP SCENARIO. SIMULATION OF THE ATR ALGORITHM IN A COMPLETE LINE WHEN ONE TRAIN IS INITIALLY DELAYED

In this scenario, a delay is applied to train 1 in **Figure 3**, and the goal is to prove the algorithm's effectiveness and to analyze the three controllers described in section V-B during the transient period until the nominal schedule is recovered. This scenario is particularly useful for evaluating the performance of the algorithm in a closed-loop configuration, that is, when the proposed algorithm has been implemented within the line simulator.

It is recalled that controller A has a low bandwidth, offering only four predesigned speed profiles: a faster speed profile that can recuperate 10 s and two slower profiles that can lose 14.7 s and 28.4 s. Besides, delay tracking and control action emission occur exclusively at platform stops, with a nominal dwell time of 20 s. On the other hand, Controllers B and C are designed for a line equipped with a continuous radio communication signalling system and high bandwidth, providing access to all speed profiles generated along the Pareto curve, where the fastest speed profile can recover 14.7 s and the slowest speed profile can lose 28.4 s.

Consequently, for the three controllers, the upper and lower running-time control action limits (URmax_k^i and URmin_k^i) are set to 28.4 s and -14.7 s respectively. Additionally, also for the three controllers, the upper and lower dwell control action limits (UPmax_k^i and UPmin_k^i) have been set to 20 s and -5 s respectively, resulting in a maximum dwell time of 20 s and a minimum dwell time of 15 s.

Unlike Controller A, delay tracking and control command emission are performed continuously, even between platforms.

The execution of running-time and dwell-time control actions has been designed in such a way that no additional delays are generated. This is achieved by selecting the speed profile that is equal to or immediately faster than the correction indicated by the algorithm.

It is important to note that in this scenario, no additional perturbations are introduced at platform stops, nominal headway is 240 s and nominal interstation running time is 100 s. Table 3 presents the weights assigned to each term in the cost function for the three controllers tested.

It is worth noting that Controller C experiences a slight loss in regulation capacity due to the more restrictive weighting of

negative running-time control actions, which are the fastest way to recover delays. For this reason, the deviation from the schedule has been slightly more penalized in the cost function with respect to the Controllers A and B.

Negative running-time and positive dwell control actions are weighted at 5 for the selected weights for the deviation with respect to the schedule and the headway. This value has been identified as suitable for this study since simulation results indicate that higher values, while increasing energy savings, excessively compromise regulation capacity. Although this configuration has been selected, it is worth noting that it can be used if the operator prefers to adopt this approach.

Conversely, lower values, closer to those in Controllers A and B, make it difficult to assess the added value of the proposed granular optimization to enhance energy efficiency.

This is demonstrated in Table 2, where it is represented, for different weights of urneg and uppos and for this synthetic closed-loop scenario, the absolute values and percentual improvements of Controller C over Controller B of the deviation from the nominal schedule (Sched), the deviation from the nominal headway (HD) and the energy consumption (E). As a reminder, Controller B uses equal weights of 0.1 for all objective function terms associated with control actions.

TABLE 2. Sensitivity analysis of controller C.

Controller C weights: Schedule: 0.3; Headway: 1; urpos, upneg: 0.1						
	urneg, uppos: 2.5		urneg, uppos: 5		urneg, uppos: 10	
Term	Absolute	Percentual over Con. B	Absolute	Percentual over Con. B	Absolute	Percentual over Con. B
Sched (s^2)	12707.31	0.03%	12641.72	0.55%	13962.22	-9.84%
HD (s^2)	11002.33	0.85%	10689.60	3.67%	10640.63	4.11%
E (kWh)	2376.26	1.18%	2341.02	2.64%	2297.36	4.46%

As a general overview, Table 3 shows the cost function weights selected for each controller.

TABLE 3. Cost function weights.

Term	Controller A	Controller B	Controller C
Schedule	0.25	0.25	0.3
Headway	1	1	1
urpos	0.1	0.1	0.1
urneg	0.1	0.1	5
uppos	0.1	0.1	5
upneg	0.1	0.1	0.1

A delay of 65 seconds is applied to train 1, with both the initial train arrangement and the line topology described in **Figure 3.** To analyze the performance of the proposed algorithm, the metrics used are the terms of the cost function (J), namely, the deviation from the nominal schedule (Sched), the deviation from the nominal headway (HD), the positive and negative run control actions (RCA+, RCA−) and positive and negative dwell-time control actions (SCA+, SCA−) executed with all previous terms squared and summed for all trains and all platforms. The slack variable has been zero for the three controllers, so they will not be analyzed.

Additionally, two more KPIs have been considered: the energy consumption (E) of the convoy to compare the three controllers in terms of both operational and energy consumption and the passenger waiting time (WT) to analyze the passenger experience and ensure that the proposed energy-efficient regulation does not lead to unacceptable delays.

This WT has been calculated using the formulation proposed by Osuna and Newell, based on the random-incidence principle and the assumptions described in [43]. The considered nominal headway for synthetic and realistic closed-loop scenarios in the main trunk is 240 s and 480 s in each branch and the demand-weighted approach, where 70% of boardings occur in the common trunk and 30% are distributed across the branches.

To see how the transient of the delays of the Controller C evolves, **Figure 6** shows the delay of the trains when they arrive and depart from the platforms for that Controller C. In Table 4, the results for the previously mentioned parameters and the energy consumption for the three controllers are presented and Table 5 shows how much Controller B has improved the performance over Controller A and Controller C over B.

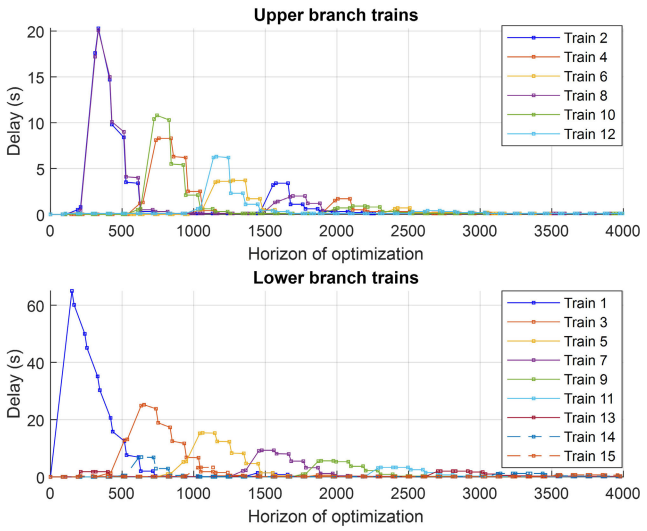

FIGURE 6. Synthetic closed-loop scenario. Controller C.

The results confirm that the proposed algorithm autonomously regulates traffic in real-time on lines with complex topology.

From the comparison of the three controllers, it can be observed that the automatic train regulation achieved by Controller A is not very precise and rather aggressive. This

TABLE 4. Synthetic closed-loop scenario results.

Term	Controller A	Controller B	Controller C
Sched (s^2)	11586.67	12711.02	12641.72
HD (s^2)	16002.91	11096.31	10689.60
RCA+ (s^2)	0.00	388.88	1135.60
RCA- (s^2)	3600.00	766.98	385.49
SCA+ (s^2)	2750.88	471.68	17.88
SCA- (s^2)	180.47	317.31	522.82
E (kWh)	2535.77	2404.57	2341.02
WT (s)	157.89	157.31	157.26

TABLE 5. Improvements in the synthetic closed-loop scenario.

Term	Controller A	Controller B
Sched (s^2)	-9.70%	0.55%
HD (s^2)	30.66%	3.67%
RCA+ (s^2)	-	-192.02%
RCA- (s^2)	78.70%	49.74%
SCA+ (s^2)	82.85%	96.21%
SCA- (s^2)	-75.82%	-64.77%
E (kWh)	5.17%	2.64%
WT (s)	0.40%	0.03%

occurs because, according to the criterion of not introducing additional delays, when the running-time control action is negative, the fastest speed profile is applied, regardless of the value of that control action. If the nominal speed profile were to be used instead, it would introduce delays larger than what the algorithm prescribes. Consequently, this leads to an earlier recovery of delays, but at the expense of significantly compromising the headway quality, which is especially critical in mass transit lines during peak hours.

For the same Controller A, it is notable that no positive running-time control actions are executed. This is because the running-time control actions generated by the algorithm are not large enough to execute the slower speed profile than the nominal, given that it is aimed at avoiding introducing additional delays. As a result, the nominal speed is executed. It is then the positive dwell-time control actions that compensate for the discrepancies between the executed running-time commands and those indicated by the algorithm. This approach, however, can lead to a passenger experience that is potentially uncomfortable.

However, since controllers B and C are equipped with high bandwidth and the ability to adjust speed profiles in real-time according to the running-time control actions issued by the algorithm, their regulation is more energy-efficient and significantly improves headway quality, which is essential for this type of complex lines. As it is evident, improving headway quality necessarily requires sacrificing schedule adherence, but as can be seen, the improvement in headway quality outweighs the slight deterioration in timetable adherence.

Additionally, a comparative analysis of the three proposed controllers reveals a synergetic relationship between energy efficiency and service quality. As shown in Table 4 and Table 5, Controller C achieves the highest energy savings (7.68% over Controller A) while simultaneously yielding lower passenger waiting time (157.21 s)

The proposed algorithm ensures that energy optimization is achieved through a more intelligent automatic train regulation rather than simply increasing dwell or running times, maintaining a service regularity that is near-ideal and the commercial speed of the line.

Finally, the study shows that the headway quality does not strongly depend on the weights of the running-time control actions; however, the schedule adherence can be somewhat affected.

C. REALISTIC CLOSED-LOOP SCENARIO. SIMULATION OF RANDOM DELAYS ON A REAL-WORLD COMPLEX TOPOLOGY LINE

In this final scenario, the system's evolution is analyzed starting from the initial configuration shown in **Figure 3**, with no initial delays, but incorporating random delays in dwell times to simulate passenger-induced disturbances. To enhance the realism of the experiment, the simulated line is based on an actual Spanish mass transit line. That is, all the running times, which are conditioned by the grades and speed limits, are taken from real data and, therefore, are different for each platform.

In this scenario, the nominal interstation travel times range between 115.7 seconds and 47.4 seconds. The nominal dwell time at platforms is 20 seconds, with the possibility of losing up to 20 seconds ($\text{UPmax}_k^i = 20s$) and recovering up to 5 seconds ($\text{UPmin}_k^i = -5s$). The upper and lower running-time control action limits (URmax_k^i and URmin_k^i) are consequent to the fastest and slowest speed profile for each interstation. The cost function weights are identical to those listed in Table 3.

Random delays were generated using a log-normal distribution with a mean of 2 seconds and a standard deviation of 1.2 seconds, consistent with methodologies employed in other studies, such as [44], to model the aleatory delays due to passengers' perturbations. To ensure a fair comparison among the three controllers, a common random seed was used so that the delay values remain identical across all cases.

Table 6 shows how much Controller B has improved the performance over Controller A and Controller C over B. **Figure 7** illustrates the evolution of the average continuous delay experienced by the trains.

The main result indicates that the proposed algorithm is highly effective in real-world line operations. Although severe random delays occur during the initial phase of the journey, the average delays over the time horizon converge to the statistical characteristics of the implemented distribution.

Since Controller A only permits speeds lower than the nominal value and is constrained by the criterion of not

TABLE 6. Improvements in real closed-loop scenario.

Term	Controller A	Controller B
Sched (s^2)	-18.99%	1.89%
HD (s^2)	29.62%	-0.77%
RCA+ (s^2)	-67.49%	-95.58%
RCA- (s^2)	11.17%	68.39%
SCA+ (s^2)	37.18%	64.20%
SCA- (s^2)	-62.12%	-59.22%
E (kWh)	4.77%	5.89%
WT (s)	5.72%	-0,11%

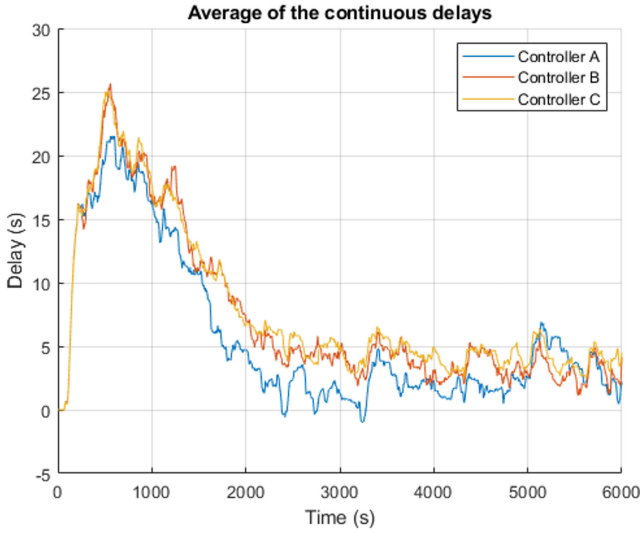

FIGURE 7. Scenario 3.

introducing additional delays, it understandably performs better in maintaining schedule adherence. However, Controllers B and C achieve approximately a 30% improvement in maintaining the nominal headway, which is highly beneficial for the operation of such lines.

As shown in Table 6, although Controller C is specifically tuned for maximum energy efficiency, the proposed model achieves a 5.61% global reduction in waiting time. However, its impact is most significant in the common trunk, where the improvement reaches 7.8 %. This localized efficiency is critical for operational stability, mitigating train bunching and station overcrowding in congested areas.

The fact that Controller C yields the highest energy savings (10.37% over Controller A) while reducing passenger waiting time confirms that the proposed model is resilient enough to handle the inherent unpredictability of daily mass-transit operations without compromising the passenger experience or the commercial speed of the line.

VII. CONCLUSION

This paper proposes a novel predictive Automatic Train Regulation algorithm designed for complex mass transit line topologies. Unlike previous approaches that focus on traffic scheduling or post-disruption traffic rescheduling, this algorithm enables real-time automatic regulation of train movement under moderate disturbances, specifically tailored to urban lines with bifurcations and intermediate short-turnings.

A central innovation of the algorithm lies in the modeling of short-turning and bifurcation nodes, which enables issuing optimized regulation commands throughout the line, even when not all trains follow the same route. By leveraging continuous communication systems, the model adapts to dynamic operational conditions, taking into account both signalling constraints and delay propagation. Furthermore, the model decomposes control actions into positive and negative components for both running and stopping phases, enabling a detailed cost function that balances headway adherence, schedule recovery, and energy consumption.

Simulation results highlight the practical advantages of the approach under realistic operational conditions, including stochastic dwell-time delays. Compared to traditional regulation systems, the proposed algorithm improves adherence to the nominal headway by almost 30%. Furthermore, it is demonstrated that this increased regularity directly translates into a 7.80% reduction in average passenger waiting time in congested areas. This enhancement is especially relevant for high-frequency railway systems where passenger satisfaction and network stability depend on headway regularity. Furthermore, the energy-efficient regulation strategy achieved through asymmetric penalization of control actions results in a 10.37% reduction in total energy consumption. These findings prove that the proposed MPC framework successfully harmonizes environmental impact with operational robustness, ensuring that energy savings do not compromise the passenger experience in complex topology lines.

ACKNOWLEDGMENT

The views and opinions expressed are however those of the authors only and do not necessarily reflect those of European Union or Europe's Rail Joint Undertaking. Neither European Union nor the granting authority can be held responsible for them.

REFERENCES

[1] S. Watanabe, Y. Sato, T. Koseki, T. Mizuma, R. Tanaka, Y. Miyaji, and E. Isobe, "Verification of optimized energy-saving train scheduling utilizing automatic train operation system," *IEEJ J. Ind. Appl.*, vol. 9, no. 2, pp. 193–200, 2020, doi: 10.1541/ieejjia.9.193.

[2] Y. S. Byun and R. G. Jeong, "Optimization of speed profiles and time schedule of the urban rail transit for energy-efficient operation," *IEEE Access*, vol. 11, pp. 146030–146041, 2023, doi: 10.1109/ACCESS.2023.3345879.

[3] B. Mo, M. Y. Von Franque, H. N. Koutsopoulos, J. P. Attanucci, and J. Zhao, "Impact of unplanned long-term service disruptions on urban public transit systems," *IEEE Open J. Intell. Transp. Syst.*, vol. 3, pp. 551–569, 2022, doi: 10.1109/OJITS.2022.3199108.

[4] J. Liu, J. Di, X. Hu, and Y. Liu, "Understanding and assessing the impact of hazardous weather on railway operations," in *Proc. IEEE 27th Int. Conf. Intell. Transp. Syst. (ITSC)*, Sep. 2024, pp. 236–241, doi: 10.1109/ITSC58415.2024.10920045.

[5] J. Yin, X. Ren, S. Su, F. Yan, and T. Tao, "Resilience-oriented train rescheduling optimization in railway networks: A mixed integer programming approach," *IEEE Trans. Intell. Transp. Syst.*, vol. 24, no. 5, pp. 4948–4961, May 2023, doi: 10.1109/TITS.2023.3236004.

[6] S. Zhang, Y. Cheng, K. Chen, C. Ma, J. Wei, and X. Hu, "A general metro timetable rescheduling approach for the minimisation of the capacity loss after random line disruption," *Transportmetrica A, Transp. Sci.*, vol. 20, no. 3, Sep. 2024, Art. no. 2204965, doi: 10.1080/23249935.2023.2204965.

[7] G. Lu, H. Zhang, Z. Shen, and X. Liu, "Refining arrival headway for high-speed trains approaching a large railway station: A speed profile intervention approach," *Railway Eng. Sci.*, vol. 33, no. 3, pp. 496–520, Sep. 2025, doi: 10.1007/s40534-024-00361-5.

[8] Y. Hou, C. Wen, P. Huang, L. Fu, and C. Jiang, "Delay recovery model for high-speed trains with compressed train dwell time and running time," *Railway Eng. Sci.*, vol. 28, no. 4, pp. 424–434, Dec. 2020, doi: 10.1007/s40534-020-00225-8.

[9] Z. Wang, E. Quaglietta, M. G. P. Bartholomeus, and R. M. P. Goverde, "Assessment of architectures for automatic train operation driving functions," *J. Rail Transp. Planning Manage.*, vol. 24, Dec. 2022, Art. no. 100352, doi: 10.1016/j.jrtpm.2022.100352.

[10] S. Li, X. Zhou, L. Yang, and Z. Gao, "Automatic train regulation of complex metro networks with transfer coordination constraints: A distributed optimal control framework," *Transp. Res. B, Methodol.*, vol. 117, pp. 228–253, Nov. 2018, doi: 10.1016/j.trb.2018.09.001.

[11] Z. Pang, L. Wang, S. Wang, L. Li, and Q. Peng, "Dynamic train dwell time forecasting: A hybrid approach to address the influence of passenger flow fluctuations," *Railway Eng. Sci.*, vol. 31, no. 4, pp. 351–369, Dec. 2023, doi: 10.1007/s40534-023-00311-7.

[12] B. Nie and Y. Tong, "A survey of applications of model predictive control to rail traffic regulation," in *Proc. China Autom. Congr. (CAC)*, Nov. 2022, pp. 2461–2465, doi: 10.1109/CAC57257.2022.10054712.

[13] X. Wang, K. Xing, and J. Wang, "Stability-enhanced model predictive control for urban rail transit train," *IEEE Access*, vol. 12, pp. 52302–52314, 2024, doi: 10.1109/ACCESS.2024.3386855.

[14] Y. Wang, Z. Liao, T. Tang, and B. Ning, "Train scheduling and circulation planning in urban rail transit lines," *Control Eng. Pract.*, vol. 61, pp. 112–123, Apr. 2017, doi: 10.1016/j.conengprac.2017.02.006.

[15] S. Li, B. De Schutter, L. Yang, and Z. Gao, "Robust model predictive control for train regulation in underground railway transportation," *IEEE Trans. Control Syst. Technol.*, vol. 24, no. 3, pp. 1075–1083, May 2016, doi: 10.1109/TCST.2015.2480839.

[16] F. Shang, J. Zhan, and Y. Chen, "Energy-saving train regulation for metro lines using distributed model predictive control," *Energies*, vol. 13, no. 20, p. 5483, Oct. 2020, doi: 10.3390/en13205483.

[17] H. Zhang, S. Li, and L. Yang, "Real-time optimal train regulation design for metro lines with energy-saving," *Comput. Ind. Eng.*, vol. 127, pp. 1282–1296, Jan. 2019, doi: 10.1016/j.cie.2018.02.019.

[18] B. Jin, X. Feng, Q. Wang, and P. Sun, "Real-time train regulation method for metro lines with substation peak power reduction," *Comput. Ind. Eng.*, vol. 168, Jun. 2022, Art. no. 108113, doi: 10.1016/j.cie.2022.108113.

[19] B. Moaveni and M. Karimi, "Subway traffic regulation using model-based predictive control by considering the passengers dynamic effect," *Arabian J. Sci. Eng.*, vol. 42, no. 7, pp. 3021–3031, Jul. 2017, doi: 10.1007/s13369-017-2508-0.

[20] Y. Yatziv and J. Haddad, "Real-time train regulation with passenger flow control in urban rail systems," *Transp. Res. C, Emerg. Technol.*, vol. 179, Oct. 2025, Art. no. 105223, doi: 10.1016/j.trc.2025.105223.

[21] Y. Yuan, S. Li, L. Yang, and Z. Gao, "Nonlinear model predictive control to automatic train regulation of metro system: An exact solution for embedded applications," *Automatica*, vol. 162, Apr. 2024, Art. no. 111533, doi: 10.1016/j.automatica.2024.111533.

[22] S. Li, L. Yang, and Z. Gao, "Efficient real-time control design for automatic train regulation of metro loop lines," *IEEE Trans. Intell. Transp. Syst.*, vol. 20, no. 2, pp. 485–496, Feb. 2019, doi: 10.1109/TITS.2018.2815528.

[23] X. Luo, T. Tang, K. Li, and H. Liu, "Computation-efficient distributed MPC for dynamic coupling of virtually coupled train set," *Control Eng. Pract.*, vol. 145, Apr. 2024, Art. no. 105846, doi: 10.1016/j.conengprac.2024.105846.

[24] Y. Oh, H.-C. Kwak, and S. Kang, "Development of optimal real-time metro operation strategy minimizing total passenger travel time and train energy consumption," *IET Intell. Transp. Syst.*, vol. 18, no. 12, pp. 2440–2458, Dec. 2024, doi: 10.1049/itr2.12582.

[25] V. N. Shmal and L. R. Aysina, "Search for the optimal solution for assigning suburban-urban trains on branched lines on each of the possible routes," *T-Comm*, vol. 14, no. 11, pp. 39–45, 2020, doi: 10.36724/2072-8735-2020-14-11-39-45.

[26] T. Schettini, M. Gendreau, O. Jabali, and F. Malucelli, "A pattern-based timetabling strategy for a short-turning metro line," *Public Transp.*, vol. 16, no. 1, pp. 1–37, Mar. 2024, doi: 10.1007/s12469-023-00339-2.

[27] F. Yuan, H. Sun, C. Zhu, and W. Deng, "Integration optimization of commuter metro lines: Train timetable, passenger flow control strategy and short-turning scheme," *Comput. Ind. Eng.*, vol. 213, Mar. 2026, Art. no. 111768, doi: 10.1016/j.cie.2025.111768.

[28] R. Zhang, M. Yang, M. Zhang, H. Li, and R. Peng, "Train service replanning in urban rail transit system: An integrated operation mode that combines express/local and short-turning strategies," *Comput. Ind. Eng.*, vol. 203, May 2025, Art. no. 111018, doi: 10.1016/j.cie.2025.111018.

[29] C. Gong, X. Luan, L. Yang, J. Qi, and F. Corman, "Integrated optimization of train timetabling and rolling stock circulation problem with flexible short-turning and energy-saving strategies," *Transp. Res. C, Emerg. Technol.*, vol. 166, Sep. 2024, Art. no. 104756, doi: 10.1016/j.trc.2024.104756.

[30] Y. Zhou and X. Tao, "Robust safety monitoring and synergistic operation planning between time- and energy-efficient movements of high-speed trains based on MPC," *IEEE Access*, vol. 6, pp. 17377–17390, 2018, doi: 10.1109/ACCESS.2018.2815643.

[31] C. K. Salode and P. Ramamoorthy, "Train timetabling with rolling stock assignment, short-turning and skip-stop strategy for a bidirectional metro line," Social Science Research Network, Rochester, NY, USA, Tech. Rep. 4789551, Apr. 2024, doi: 10.2139/ssrn.4789551.

[32] D. Bauso, C. Fecarotti, and A. Khaleghi, "Cooperative control and stability analysis for virtual coupling of rail vehicles," *Control Eng. Pract.*, vol. 133, Apr. 2023, Art. no. 105452, doi: 10.1016/j.conengprac.2023.105452.

[33] Z. Ning, D. Ou, C. Xie, L. Zhang, B. Gao, and J. He, "Optimal convoy composition for virtual coupling trains at junctions: A coalition formation game approach," *Transp. Res. C, Emerg. Technol.*, vol. 154, Sep. 2023, Art. no. 104277, doi: 10.1016/j.trc.2023.104277.

[34] C. Luo, Y. Liu, Y. Li, Z. Sun, X. Hu, and J. Liu, "Dynamic decoupling control for virtually coupled train set: A reinforcement learning-based model predictive control approach," in *Proc. IEEE 27th Int. Conf. Intell. Transp. Syst. (ITSC)*, Sep. 2024, pp. 242–247, doi: 10.1109/ITSC58415.2024.10920128.

[35] M. Zhang, Y. Wang, S. Su, T. Tang, and B. Ning, "A short turning strategy for train scheduling optimization in an urban rail transit line: The case of Beijing subway line 4," *J. Adv. Transp.*, vol. 2018, pp. 1–19, Aug. 2018, doi: 10.1155/2018/5367295.

[36] D. He, Y. He, L. Zhang, Y. Chen, Z. Sun, and J. Miao, "Train operation scheme of short-turning routing in urban rail transit based on passenger travel," *Transp. Res. Record: J. Transp. Res. Board*, vol. 2678, no. 12, pp. 2125–2139, Dec. 2024, doi: 10.1177/03611981231167428.

[37] S. Li, R. Xu, and K. Han, "Demand-oriented train services optimization for a congested urban rail line: Integrating short turning and heterogeneous headways," *Transportmetrica A, Transp. Sci.*, vol. 15, no. 2, pp. 1459–1486, May 2019, doi: 10.1080/23249935.2019.1608475.

[38] *FP1-MOTIONAL*. Accessed: Jan. 19, 2026. [Online]. Available: https://rail-research.europa.eu/rail-projects/fp1-motional/

[39] V. Van Breusegem, G. Campion, and G. Bastin, "Traffic modeling and state feedback control for metro lines," *IEEE Trans. Autom. Control*, vol. 36, no. 7, pp. 770–784, Jul. 1991, doi: 10.1109/9.85057.

[40] A. Fernandez, A. P. Cucala, B. Vitoriano, and F. de Cuadra, "Predictive traffic regulation for metro loop lines based on quadratic programming," *Proc. Inst. Mech. Eng., F, J. Rail Rapid Transit*, vol. 220, no. 2, pp. 79–89, Mar. 2006, doi: 10.1243/09544097f00505.

[41] Á. Cidoncha, A. Fernández-Rodríguez, A. P. Cucala, and A. Fernández-Cardador, "Predictive traffic regulation model for railway mass transit lines equipped with continuous communication systems," *IEEE Access*, vol. 12, pp. 96862–96877, 2024, doi: 10.1109/ACCESS.2024.3427314.

[42] A. Fernández-Rodríguez, A. Fernández-Cardador, A. P. Cucala, M. Domínguez, and T. Gonsalves, "Design of robust and energy-efficient ATO speed profiles of metropolitan lines considering train load variations and delays," *IEEE Trans. Intell. Transp. Syst.*, vol. 16, no. 4, pp. 2061–2071, Aug. 2015, doi: 10.1109/TITS.2015.2391831.

[43] E. E. Osuna and G. F. Newell, "Control strategies for an idealized public transportation system," *Transp. Sci.*, vol. 6, no. 1, pp. 52–72, Feb. 1972.
[44] I. Martínez, B. Vitoriano, A. Fernández-Cardador, and A. P. Cucala, "Statistical dwell time model for metro lines," *WIT Press*, vol. 96, pp. 223–232, Jun. 2007, doi: 10.2495/ut070221.

ÁLVARO CIDONCHA received the B.Sc. and M.Sc. degrees in industrial engineering from Comillas Pontifical University, Madrid, in 2022 and 2024, respectively, where he is currently pursuing the Ph.D. degree with the Railway Research Group, Institute of Research in Technology.

His research interests include train simulation, traffic control, and railway efficient operation.

ADRIÁN FERNÁNDEZ-RODRÍGUEZ received the degree in industrial engineering from Universidad Politécnica de Madrid, in 2012, and the Ph.D. degree from Comillas Pontifical University, Madrid, in 2018.

He is currently a Research Fellow with the Railway Research Group, Institute for Research in Technology, Comillas Pontifical University. His research interests include train operation modeling, energy efficiency in railways, and nature inspired optimization.

ASUNCIÓN P. CUCALA received the degree in industrial engineering and the Ph.D. degree from Comillas Pontifical University, Madrid, Spain.

She is currently the Director of the Institute for Research in Technology, a Research Fellow of the Railways Research Group, and a Full Professor with the ICAI School of Engineering, Comillas Pontifical University. Her research interests include train simulation, railway operation and control, energy efficiency in railways, and railway capacity analysis.

ANTONIO FERNÁNDEZ-CARDADOR received the degree in physics from Universidad Complutense, Madrid, Spain, and the Ph.D. degree from Comillas Pontifical University, Madrid.

He is currently a Research Fellow with the Railways Research Group, Institute for Research in Technology, and a Full Professor with the ICAI School of Engineering, Comillas Pontifical University. His research interests include train simulation, railway operation and control, eco-driving, and railway capacity.

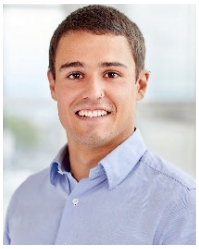

JORGE GOROSTIZA-HERRERO received the B.Sc. degree in aerospace engineering and the M.Sc. degree in aeronautical engineering from the Technical University of Madrid (UPM), Spain, in 2016 and 2018, respectively.

He is currently a CBTC Software Engineer with the CAF Signalling. His main areas of interests include the modeling and simulation of train dynamics, as well as the design and implementation of algorithms for railway traffic regulation applications.